PARAMETER CONSIDERATIONS FOR THE RETRIEVAL OF SURFACE SOIL MOISTURE FROM SPACEBORNE GNSS-R

J.F. Munoz-Martin[1], R. Onrubia[1], D. Pascual[1], H. Park[1], A. Camps[1],
C. Rüdiger[2], J. P. Walker[2], and A. Monerris[3]

[1]CommSensLab - UPC, Universitat Politècnica de Catalunya – BarcelonaTech, and IEEC/CTE-UPC, 08034 Barcelona, Spain
[2]Department of Civil Engineering, Monash University, Clayton, VIC 3800, Australia
[3]Department of Infrastructure Engineering, The University of Melbourne, Parkville, VIC 3010, Australia,
e-mail: joan.francesc@tsc.upc.edu, camps@tsc.upc.edu

ABSTRACT

The Microwave Interferometric Reflectometer (MIR) is an airborne GNSS-R instrument developed by Universitat Politècnica de Catalunya. In 2018, it was flown twice over the agricultural Yanco area, New South Wales, Australia, once after a very dry period, and a further time the day after a strong rain event. This rain event resulted in many crop fields being entirely flooded, producing a saturation in the GNSS-R reflectivity value. In this work, the received data set is processed to identify the optimum integration time withthe goal to minimize pixel blurring. This issue is assessed for airborne conditions, and then extra-polated to the spaceborne case. The presented results show that the blurring of the GNSS waveform is produced even from an airborne sensor with short integration times. Following the determination of an optimal integration time for the platform in use, the surface roughness term in the reflectivity equation can be isolated due to the signal saturation during very wet surface conditions. The final results from the two channels (L1 C/A and L5) are subsequently presented. In this case, it is shown that most reflectivity variations in GNSS-R measurements are linked to surface roughness and Speckle noise fluctuations rather than soil moisture changes.

Index Terms— GNSS-R, roughness, soil moisture

1. INTRODUCTION

Soil moisture is a key geophysical parameter in the water cycle. Data from NASA's CyGNSS mission [1, 2] has proven that GNSS-R can be used to estimate soil moisture from space following different approaches (Table 1 from [3]), such as using time series [4], averaging multiple measurements [5] in lower resolution cells (i.e. 36 km), or using artificial neu- ral networks (ANN) [6, 7], which can provide a higher spa- tial resolution. However, none of the algorithms provides the maximum achievable spatial resolution from Global Navigation Satellite System - Reflectometry (GNSS-R): ~ 500 m, the size of the first Fresnel zone from space. Most algorithms make us of either spatial or temporal averaging, which limits the spatial resolution of the GNSS-R product. This effect is observable across other remote sensor technologies such as microwave radiometry, where an increase in the spatial resolution leads to a decrease of the radiometric sensitivity (i.e. larger noise).

The GNSS-R limitations for soil moisture retrieval using data from a single-pass are discussed in [8], where even measuring the surface roughness and the vegetation in situ (i.e. using a laser profiler and a multi-spectral imager), it was impossible to retrieve surface soil moisture analytically. Furthermore, the level of soil moisture also affects the penetration depth of the GNSS signal [9], and therefore the effective surface roughness varies with soil moisture, as well as with frequency, and other factors. As a function of where in the soil layer the reflection takes place, the effect of the surface roughness can provide a signal drop of up to 18 dB, for a local RMS surface height up to 4 cm using [10]:

$$\Gamma(\vartheta) = R(\vartheta)^2 \gamma^2 exp(-4k^2\sigma_h^2 cos^2(\vartheta)), \quad (1)$$

where Γ is the reflectivity, R is the amplitude of the Fresnel reflection coefficient, ϑ is the local incidence angle, γ accounts for the vegetation attenuation, k is the wave number (i.e. $2\pi/\lambda$), and σ_h is the RMS surface height.

2. INTEGRATION TIME CONSIDERATIONS

To address the issue discussed above from a different perspective, GNSS-R data collected by the Microwave Interferometer Reflectometer (MIR) is analyzed here. MIR is a dual-band (L1 and L5) GNSS reflectometer that was designed to work as interferometric GNSS-R [11], but raw data is sampled at 32 MS/s, and stored at 1 bit [12]. The data set selected to conduct this analysis comprises one flight over Yanco, Australia, 2018. The flight took place on May 1st, the day after a

strong rain event, where the average soil moisture was ~0.27-0.33 m^3/m^3 [13]. The region is constantly monitored by the OzNet hydrological monitoring network [14], and the flight was carried out at an altitude h = 500 m, and at a velocity v_{plane} = 75 m/s.

One of the fixed parameters of different GNSS-R sensors is the incoherent integration time. One second of incoherent integration is typically used in the airborne case [8], but also in the spaceborne one, e.g. SGR-ReSi instrument of TDS-1 [15], CyGNSS [1], or the BuFeng-1 mission [16]. This large integration time has been discussed in [17, 18], and it seems that it is an order of magnitude above the limit to prevent the auto-correlation function to be blurred if no retracking is implemented. However, it has been proven that using shorter integration times is key for the retrieval of other geophysical parameters, such as swell waves [19].

To assess the impact of different integration times, the complex waveform of the reflected signal has been retrieved at 1 ms coherent integration time for both L1 C/A and L5 signals. Up to 1 second of complex waveforms are appended in a vector, and the covariance matrix computed in the T_{int} axis. Note that N is the number of 1 ms coherently integrated segments used to generate the covariance matrix (i.e. T_{int} = 1000 ms means N = 1000).

Figures 1 and 2 show the covariance matrices at L1and L5 respectively for three different integration times: T_{int} =100, 200, and 1000 ms.

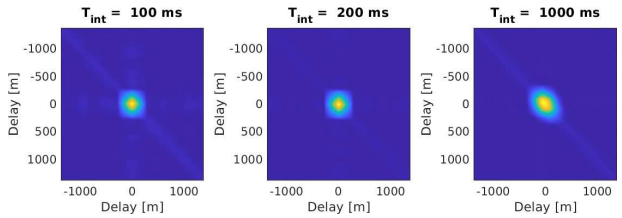

Fig. 1: Covariance matrices at L1 C/A at three integration times, 100, 200, and 1000 ms. The delay axes corresponds to the code displacement in meters, converted from the 1-sample displacement (in seconds) multiplied the sampling rate (Hz) and by the speed of light (m).

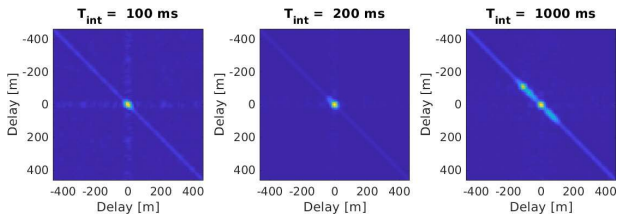

Fig. 2: Covariance matrices at L5 at three integration times, 100, 200, and 1000 ms.

As it can be seen, longer integration times produce a blurring in the L1 C/A waveform, and even the appearance of multiple peaks in the L5 waveform. In the airborne case, the blurring is produced by two effects: the change in the small scale of the facets that produce the reflection, and the blurring of the waveform due to chip length. The first one is mitigated by having an integration time smaller than the chip length over the platform velocity according to Eq. 2.

$$T_{int_{max}} = \frac{L_{chip}}{v_{platform}}. \quad (2)$$

The second effect depends on the size of the first Fres- nel zone (l_{Fr}), where the specular reflection occurs. In the airborne case flying at h = 500 m, this is l_{Fr} ~ 10 m. Therefore, the maximum integration time to prevent multiple Fresnel zones to *overlap* for L1 C/A is 130 ms. In the L5 case,the blurring starts to appear at 100 ms, and the waveform is almost unrecognizable for longer integration times (i.e. 1000 ms). Similarly, this is also occurring when the GNSS-R receiver moves more than the size of the first Fresnel zone.

Applying the same reasoning for the satellite case, the first Fresnel zone is always larger than 300 m in L1 C/A and 30 m in L5. Therefore, for the spaceborne case the maximum integration time is limited by the platform velocity as in Eq. 2, and introduced in [17, 18]. In this case, 40 ms for L1 C/A and 4 ms for L5 signals. Therefore, in a generic way, the maximum integration time will be set by Eq. 3.

$$T_{int_{max}} = \frac{min\{L_{chip}, L_{Fr}\}}{v_{platform}}. \quad (3)$$

3. SURFACE ROUGHNESS IMPACT IN SOIL MOISTURE RETRIEVAL

Despite choosing the most appropriate integration time for the current setting, the non-blurred reflection is still affected by the signal fading produced by the random phase introduced by each of the scatterers across the rough surface. This attenuation is the unresolved unknown in Eq. 1 that needs to be compensated for in order to analytically compute the soil moisture from the reflectivity. To assess this problem, data over a crop field with a Normalized Difference Vegetation Index of 0.2-0.3 has been selected. Figure 3 shows the probability density function (PDF) of the reflectivity of the area under study.

Following [10], and from the analysis of this flight in [13], the reflectivity values are saturated because of the high soil moisture values. Therefore, the variability in the reflectivity values seen in Fig. 3 is mostly produced by the surface roughness effect, and not by soil moisture variations.

As it can be seen, despite the reflectivity should be saturated because of high soil moisture values, it is not the case, and the responsible is the surface roughness.

A saturated reflectivity Γ -5 dB (i.e. average reflectiv- ity plus 1 sigma of the PDF in Fig. 3) is considered for both

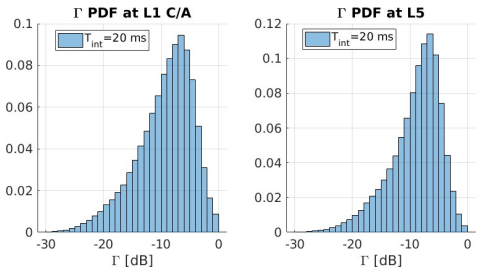

Fig. 3: Reflectivity PDF over the area of study calculated at T_{int} = 20 ms.

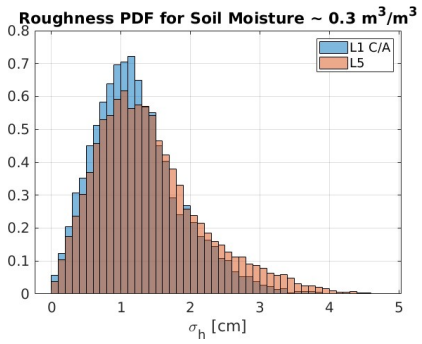

Fig. 4: Surface roughness estimation at L1 C/A using T_{int} = 20 ms.

L1 C/A and L5 signals, and σ_h is isolated from Eq. 1. Assuming a negligible vegetation attenuation $\kappa \approx 0$, σ_h can be computed for each incidence angle, as shown in Fig. 4.

Accordingly, the average surface roughness (σ_h) is 1.23 cm at L1 C/A and 1.4 cm at L5. Surface roughness values up to 4 cm are derived from this computation, which means an attenuation up to 18 dB. In this case, the impact of a large surface roughness led to incorrectly retrieved soil moisture values. Therefore, a wet area could be identified as dry because of the large local surface roughness. The only way to get rid of this effect is, as shown in [3], to perform a spatio-temporal averaging of the reflectivity in order to "smooth" the surface roughness to a biased value.

In [13], the effect of increasing the averaging time is studied using an ANN as the soil moisture recovery algorithm. Results show that there is a clear trade-off between the spatial resolution and the radiometric sensitivity. As seen in Fig. 5 (adapted from [13]), an increase in the averaging time leads to a poorer spatial resolution, but a much better radiometric sensitivity. Moreover, the use of additional statistical parameters, such as the standard deviation of the reflectivity, shows a certain level of correlation as a proxy to correct the roughness and the Speckle noise ([3, 13]) of the reflectivity values.

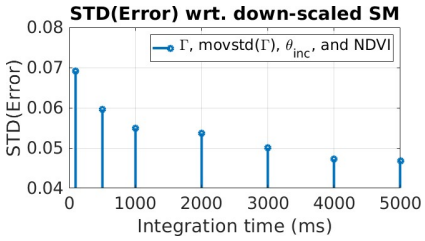

Fig. 5: Standard deviation of the error of the ANN retrieval algorithm of MIR with respect to 20 m Sentinel-2/SMOS downscaled soil moisture product.

4. CONCLUSIONS

This work has presented the effect of increasing the integration time in both L1 C/A and L5 GPS signals, reaching a limit where re-tracking is required. This limit depends on either the first Fresnel zone or the signal chip length. Whicheveris smaller sets the limit for the integration time without re-tracking. Despite setting the optimum integration time, the non-blurred waveform is still significantly affected by the surface roughness. In this case, assuming a constant reflectivity because of the saturated soil moisture content, the reflectivity variability is linked to the surface roughness, which can be estimated, and compensated for to obtain a good soil moisture estimate. Results will be presented at the conference.

5. ACKNOWLEDGEMENTS

This work has been (partially) sponsored by project SPOT: Sensing with Pioneering Opportunistic Techniques grant RTI2018-099008-B-C21 / AEI / 10.13039/501100011033, and by the Unidad de Excelencia Maria de Maeztu MDM-2016-0600, and by the grant for recruitment of early-stage research staff FI-DGR 2018 of the AGAUR - Generalitat de Catalunya (FEDER), Spain.

6. REFERENCES

[1] C. S. Ruf, S. Gleason, Z. Jelenak, S. Katzberg, A. Ridley, R. Rose, J. Scherrer, and V. Zavorotny, "The CYGNSS nanosatellite constellation hurricane mission," in *International Geoscience and Remote Sensing Symposium (IGARSS)*. IEEE, jul 2012, pp. 214–216. [Online]. Available: http://ieeexplore.ieee.org/lpdocs/epic03/wrapper.htm?arnumber=6351600

[2] C. Ruf, M. Clarizia, S. Gleason, Z. Jelenak, J. Murray, M. Morris, S. Musko, D. Posselt, D. Provost, D. Starkenburg, and V. Zavorotny, *CYGNSS Handbook*, digital ed. Ann Arbor, MI: Michigan Pub., 2016.

[3] Q. Yan, W. Huang, S. Jin, and Y. Jia, "Pan-tropical soil moisture mapping based on a three-layer model

from CYGNSS GNSS-R data," *Remote Sensing of Environment*, vol. 247, p. 111944, Sep. 2020. [Online]. Available: https://doi.org/10.1016/j.rse.2020.111944

[4] M. M. Al-Khaldi, J. T. Johnson, A. J. O'Brien, A. Balenzano, and F. Mattia, "Time-Series Retrieval of Soil Moisture Using CYGNSS," *IEEE Transactions on Geoscience and Remote Sensing*, vol. 57, no. 7, pp. 4322–4331, 2019.

[5] M. P. Clarizia, N. Pierdicca, F. Costantini, and N. Floury, "Analysis of CYGNSS Data for Soil Moisture Retrieval," *IEEE Journal of Selected Topics in Applied Earth Observations and Remote Sensing*, vol. 12, no. 7, pp. 2227–2235, 2019.

[6] O. Eroglu, M. Kurum, D. Boyd, and A. C. Gurbuz, "High spatio-temporal resolution CYGNSS soil moisture estimates using artificial neural networks," *Remote Sensing*, vol. 11, no. 19, p. 2272, Sep. 2019. [Online]. Available: https://doi.org/10.3390/rs11192272

[7] V. Senyurek, F. Lei, D. Boyd, M. Kurum, A. C. Gurbuz, and R. Moorhead, "Machine learning-based CYGNSS soil moisture estimates over ISMN sites in CONUS," *Remote Sensing*, vol. 12, no. 7, p. 1168, Apr. 2020. [Online]. Available: https://doi.org/10.3390/rs12071168

[8] A. Camps, H. Park, J. Castellv´ı, J. Corbera, and E. Ascaso, "Single-pass soil moisture retrievals using GNSS-R: Lessons learned," *Remote Sensing*, vol. 12, no. 12, p. 2064, Jun. 2020. [Online]. Available: https://doi.org/10.3390/rs12122064

[9] F. Li, X. Peng, X. Chen, M. Liu, and L. Xu, "Analysis of Key Issues on GNSS-R Soil Moisture Retrieval Based on Different Antenna Patterns," *Sensors*, vol. 18, no. 8, p. 2498, Aug. 2018. [Online]. Available: https://doi.org/10.3390/s18082498

[10] H. Park, A. Camps, J. Castellvi, and J. Muro, "Generic Performance Simulator of Spaceborne GNSS-Reflectometer for Land Applications," *IEEE Journal of Selected Topics in Applied Earth Observations and Remote Sensing*, vol. 13, pp. 3179–3191, 2020.

[11] V. U. Zavorotny, S. Gleason, E. Cardellach, and A. Camps, "Tutorial on remote sensing using gnss bistatic radar of opportunity," *IEEE Geoscience and Remote Sensing Magazine*, vol. 2, no. 4, pp. 8–45, Dec 2014.

[12] R. Onrubia, D. Pascual, A. Camps, A. Alonso-Arroy, and H. Park, "MIR: The microwave interferometric reflectometer, a new airborne sensor for GNSS-R advanced research," in *International Geoscience and Remote Sensing Symposium (IGARSS)*. Melbourne, Australia: IEEE, jul 2013, pp. 109–112. [Online]. Available: http://ieeexplore.ieee.org/lpdocs/epic03/wrapper.htm?arnumber=6721104

[13] J. F. Munoz-Martin, R. Onrubia, D. Pascual, H. Park, A. Camps, C. Rüdiger, J. Walker, and A. Monerris, "Single-Pass Soil Moisture Retrieval using GNSS-R at L1 and L5 bands: Results from airborne experiment," *Remote Sensing [Submitted]*, 2020.

[14] A. B. Smith, J. P. Walker, A. W. Western, R. I. Young, K. M. Ellett, R. C. Pipunic, R. B. Grayson, L. Siriwardena, F. H. S. Chiew, and H. Richter, "The Murrumbidgee soil moisture monitoring network data set," *Water Resources Research*, vol. 48, no. 7, Jul. 2012. [Online]. Available: https://doi.org/10.1029/2012wr011976

[15] P. Jales, "Spaceborne Receiver Design for Scatterometric GNSS Reflectometry," *PhD. thesis from University of Surrey*, 2012.

[16] C. Jing, X. Niu, C. Duan, F. Lu, G. Di, and X. Yang, "Sea surface wind speed retrieval from the first chinese gnss-r mission: Technique and preliminary results," *Remote Sensing*, vol. 11, no. 24, 2019. [Online]. Available: https://www.mdpi.com/ 2072-4292/11/24/3013

[17] H. Park, D. Pascual, A. Camps, F. Martin, A. Alonso-Arroyo, and H. Carreno-Luengo, "Analysis of Spaceborne GNSS-R Delay-Doppler Tracking," *IEEE Journal of Selected Topics in Applied Earth Observations and Remote Sensing*, vol. 7, no. 5, pp. 1481–1492, may 2014. [Online]. Available: http://ieeexplore.ieee.org/lpdocs/epic03/wrapper.htm?arnumber=6820734

[18] A. Camps, H. Park, E. Valencia i Domenech, D. Pascual, F. Martin, A. Rius, S. Ribo, J. Benito, A. Andres-Beivide, P. Saameno, G. Staton, M. Martin-Neira, S. DAddio, and P. Willemsen, "Optimization and Performance Analysis of Interferometric GNSS-R Altimeters: Application to the PARIS IoD Mission," *IEEE Journal of Selected Topics in Applied Earth Observations and Remote Sensing*, vol. 7, no. 5, pp. 1436–1451, may 2014. [Online]. Available: http://ieeexplore.ieee.org/lpdocs/epic03/wrapper.htm?arnumber=6817554

[19] J. F. Munoz-Martin, R. Onrubia, D. Pascual, H. Park, A. Camps, C. Rüdiger, J. Walker, and A. Monerris, "Experimental evidence of swell signatures in airborne L5/E5a GNSS-Reflectometry," *Remote Sensing*, vol. 12, no. 11, p. 1759, May 2020. [Online]. Available: https://doi.org/10.3390/rs12111759